Pergamon

Int. J. Heat Mass Transfer. Vol. 40, No. 5, pp. 1061–1070, 1997

0017-9310/97 $17.00+0.00

PII: S0017-9310(96)00158-5

Heat transfer and flow field in a pipe with sinusoidal wavy surface—I. Numerical investigation

G. RUSS and H. BEER

Institut für Technische Thermodynamik, Technische Hochschule Darmstadt, 64287 Darmstadt, Germany

(*Received* 25 *October* 1995 *and in final form* 29 *April* 1996)

Abstract—The majority of publications in the field of convective transport enhancement in conduits with wavy walls have provided the distribution of the mean Sherwood or Nusselt number per wavelength. The mechanisms, however, driving the increase in heat and mass transfer have not been clearly understood so far. This paper presents the results of a detailed numerical investigation of local heat and mass transfer enhancement in a pipe with sinusoidally varying diameter, covering a wide range of Reynolds numbers from laminar to turbulent flow. The discussion is focused on the predicted flow field and the turbulence structure, allowing a better understanding of the calculated Sherwood and Nusselt numbers. Part II of this paper deals with the experimental validation of the numerically achieved results. Copyright © 1996 Elsevier Science Ltd.

1. INTRODUCTION

A tube with a periodically converging–diverging cross section is one of several devices employed for enhancing the heat and mass transfer efficiency due to turbulence promotion. The present investigation appears to have a number of important applications such as industrial heat exchangers and chemical reactors. Furthermore, heat transfer in gas turbines, which is often enhanced by turbulence promoters and jet impingement may also be improved by installing converging–diverging sections in the internal cooling passages. In addition to any direct practical importance, flow in wavy tubes serves as a simple example of separated flow, in which the complex interactions of separated vortices, free shear layers, driving wall-bounded shear flows and the resulting heat and mass transfer can be examined in some detail.

Sparrow and Prata [1] presented numerical solutions of fully developed mass transfer at low Schmidt numbers in a tube with a triangular wavy wall for laminar flow. With experiments applying the naphthalene sublimation technique, they verified the numerical predictions of the Sherwood number. The authors found that this tube is not an attractive enhancement device for mass transfer under laminar flow conditions compared to the corresponding tube with a straight wall.

Nishimura *et al.* [2] investigated flow characteristics such as flow pattern, pressure drop and wall shear stress in a channel with a symmetric sinusoidal wavy wall. For the wavy channel used in their study laminar flow existed at Reynolds numbers less than $Re_{dm} = 350$. An increase of the Reynolds number caused turbulent flow to develop, owing to the onset of unsteady vortex motion. In the laminar flow range the friction factor was inversely proportional to the Reynolds number and in the turbulent range it was proven to be independent of the Reynolds number.

In further studies Nishimura *et al.* [3, 4] investigated the mass transfer in a wavy channel for transitional and turbulent flows and concluded that this channel yields a good mass transfer enhancement compared to the corresponding straight-walled channel. The enhancement is caused by shear layers and traveling waves which augment convective transport normal to the wall.

Greiner *et al.* [5] focused their attention on passive enhancement techniques in channel flows by shear destabilization. In these systems hydrodynamic instability modes, which normally decay in an unenhanced flow, are destabilized by careful modification of the system solid boundaries, such as cutting grooves in the channel wall. They found that the onset location of transport enhancement in the axial direction of the conduit is a function of the Reynolds number.

The purpose of this study is to examine analytically the influence of a sinusoidally varying radius on the flow regime, the turbulence structure and the local convective transport.

2. ANALYSIS

Figure 1 depicts the geometry under consideration. The axial variation of the pipe-radius is determinated by a sinus function and can be described by two non-dimensional parameters:

NOMENCLATURE

a	thermal diffusivity
A_c	cross-section
A_μ, A_t, A_{cl}	constants of turbulence model
c	mean concentration
c_p	specific heat at constant pressure
C_l	constant in Yap correction
C_1, C_2, C_μ	constants in turbulence model
d_m	mean diameter
D_{12}	diffusion coefficient
F	streamfunction
h	amplitude of the wallfunction
k	turbulent kinetic energy
l	typical length of turbulence
Nu	Nusselt number ($\alpha d_m/\lambda$)
n	coordinate normal to the wall
p	pressure
Pr	Prandtl number (ν/a)
Pr_t	turbulent Prandtl number (ν_t/ν_q)
q	heat flux
R_k, R_t	Reynolds numbers of the turbulence model
Re_{dm}	Reynolds number ($U_m d_m/\nu$)
Sc	Schmidt number (ν/D_{12})
Sc_t	turbulent Schmidt number (ν_t/ν_D)
Sh	Sherwood number ($\beta d_m/D_{12}$)
T	absolute temperature
u	velocity component in axial direction
U_m	mean axial velocity
v	velocity component in radial direction
x	axial coordinate
y	radial coordinate.

Greek symbols

α	heat transfer coefficient
β	mass transfer coefficient
γ_h, γ_Λ	dimensionless geometry parameters
δ	dimensionless distance between centerline and wall
ε	dissipation rate of the turbulent kinetic energy
η	dynamic viscosity
λ	thermal conductivity
λ_w	friction coefficient $(d_m/10\Lambda)(\Delta p/\frac{1}{2}\rho U_m^2)$
Λ	wavelength of the wallfunction
ν	kinematic viscosity
ν_t	eddy viscosity
ρ	density
σ_K, σ_ε	constants of the turbulence model
ξ	wavenumber.

Subscripts

m	average value over cross-section
W	at the wall
0	initial state, transformed coordinates.

Superscripts

*	dimensionless value
~	Mangler-coordinates
i	$i = 0$, cartesian, $i = 1$, cylindrical coordinate system.

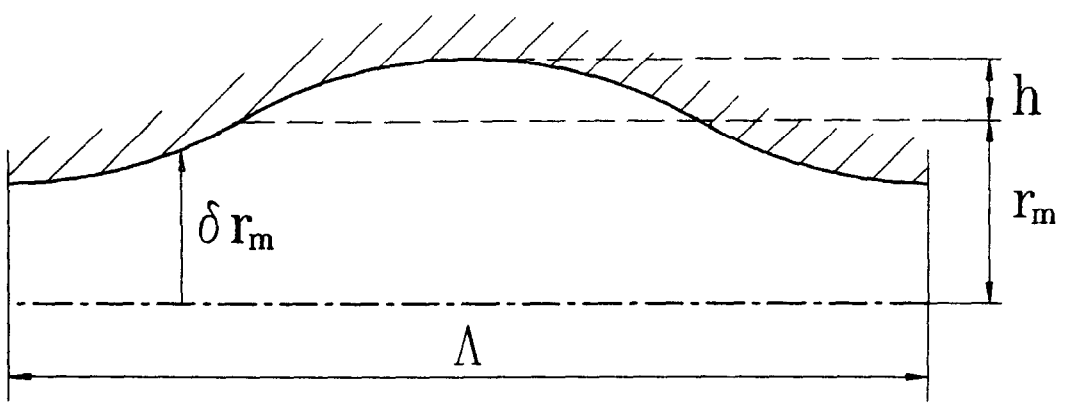

Fig. 1. Geometry under consideration.

$$\gamma_h = 2\frac{h}{d_m} \tag{1}$$

$$\gamma_\Lambda = 2\frac{\Lambda}{d_m}. \tag{2}$$

The numerical analysis is based on the time averaged conservation equations of mass, momentum and energy in an axisymmetric cylindrical coordinate system. It is assumed that the fluid is Newtonian and incompressible with constant properties. To predict

the convective mass transfer the concentration equation for a binary mixture of two non-reacting gases is solved.

In turbulent flow it is assumed that all fluid properties can be described by a time averaged and a statistically distributed portion. As an effect of these assumptions additional terms occur in the equations of motion, energy and concentration, which describe the turbulent stresses and the turbulent transport of energy and concentration. These terms are modeled with the help of the k–ε model of Lam and Bremhorst [6] by introducing a turbulent viscosity:

$$\nu_t = C_\mu \frac{k^2}{\varepsilon}. \tag{3}$$

To calculate the distribution of the turbulent kinetic energy k and the turbulent dissipation rate ε, two additional transport equations have to be solved. In contrast to the standard k–ε model, using wall functions, the low Reynolds number (LRN) model of Lam and Bremhorst scales the constants in the transport equations as functions f_μ, f_1, f_2 of the normal distance to the wall and two additional turbulent Reynolds numbers to account for the turbulence structure in the near wall region:

$$Re_k = \frac{\sqrt{k}n}{\nu} \tag{4}$$

$$Re_t = \frac{k^2}{\nu\varepsilon} \tag{5}$$

$$f_\mu = (1 - e^{-A_\mu Re_k})^2 \left(1 + \frac{A_t}{Re_t}\right) \tag{6}$$

$$f_1 = 1 + \left(\frac{A_{c1}}{f_\mu}\right)^3 \tag{7}$$

$$f_2 = 1 - e^{-Re_t^2}. \tag{8}$$

For ν_t the following equation holds:

$$\nu_t = f_\mu C_\mu \frac{k^2}{\varepsilon}. \tag{9}$$

To reduce computer storage and time, the boundary-layer assumptions were used. If δ describes the local thickness of the boundary-layer, L the typical length of the problem and u, v the velocity components in the x, y direction, the boundary-layer assumption can be applied under the conditions:

$$\frac{1}{\sqrt{Re}} = \varepsilon_s \ll 1 \quad \frac{\delta}{L} = 0(\varepsilon_s) \quad \frac{v}{u} = 0(\varepsilon_s) \tag{10}$$

and

$$\frac{\partial^2}{\partial x^2} \ll \frac{\partial^2}{\partial y^2}. \tag{11}$$

With these restrictions the following set of equations has to be solved:

$$\frac{\partial u}{\partial x} + \frac{1}{y^j}\frac{\partial (y^j v)}{\partial y} = 0 \tag{12}$$

$$u\frac{\partial u}{\partial x} + v\frac{\partial u}{\partial y} = -\frac{1}{\rho}\frac{\partial p}{\partial x} + \frac{1}{y^j}\frac{\partial}{\partial y}\left[y^j(\nu + \nu_t)\frac{\partial u}{\partial y}\right] \tag{13}$$

$$\frac{\partial p}{\partial y} = 0 \tag{14}$$

$$u\frac{\partial k}{\partial x} + v\frac{\partial k}{\partial y} = \frac{1}{y^j}\frac{\partial}{\partial y}\left[y^j\left(\nu + \frac{\nu_t}{\sigma_K}\right)\frac{\partial k}{\partial y}\right] + \nu_t\left(\frac{\partial u}{\partial y}\right)^2 - \varepsilon \tag{15}$$

$$u\frac{\partial \varepsilon}{\partial x} + v\frac{\partial \varepsilon}{\partial y} = \frac{1}{y^j}\frac{\partial}{\partial y}\left[y^j\left(\nu + \frac{\nu_t}{\sigma_\varepsilon}\right)\frac{\partial \varepsilon}{\partial y}\right] + f_1 C_1 \frac{\varepsilon}{k}\nu_t\left(\frac{\partial u}{\partial y}\right)^2 - f_2 C_2 \frac{\varepsilon^2}{k} \tag{16}$$

$$u\frac{\partial T}{\partial x} + v\frac{\partial T}{\partial y} = \frac{1}{y^j}\frac{\nu}{Pr}\frac{\partial}{\partial y}\left[y^j\left(1 + \frac{Pr}{Pr_t}\frac{\nu_t}{\nu}\right)\frac{\partial T}{\partial y}\right] \tag{17}$$

$$u\frac{\partial c}{\partial x} + v\frac{\partial c}{\partial y} = \frac{1}{y^j}\frac{\nu}{Sc}\frac{\partial}{\partial y}\left[y^j\left(1 + \frac{Sc}{Sc_t}\frac{\nu_t}{\nu}\right)\frac{\partial c}{\partial y}\right] \tag{18}$$

with the following boundary conditions: at the wall

$$u = 0 \quad v = 0 \quad k = 0 \quad \varepsilon = \nu\left(\frac{\partial^2 k}{\partial y^2}\right) \tag{19}$$

$$T = T_w \quad c = c_w \tag{20}$$

on the centerline

$$\frac{\partial u}{\partial y} = 0 \quad \frac{\partial k}{\partial y} = 0 \quad \frac{\partial \varepsilon}{\partial y} = 0, \quad \frac{\partial v}{\partial y} = 0 \quad \frac{\partial T}{\partial y} = 0 \quad \frac{\partial c}{\partial y} = 0 \tag{21}$$

and with the standard set of constants

$$C_1 = 1.44 \quad C_2 = 1.92 \quad C_\mu = 0.09$$
$$\sigma_K = 1.0 \quad \sigma_\varepsilon = 1.3. \tag{22}$$

In addition the continuity equation must be met:

$$U_m A_c = \int_{A_c} u(y)\,d\tilde{A}. \tag{23}$$

Due to the lack of the axial diffusion term, the above equations are normally not valid in regions with flow reversal. However, Anderson *et al.* [7] recommended the use of boundary-layer equations in regions with reversed flow as well, as long as the separation bubble is closed and not too large. Since the recirculation zones in the pipe under consideration are expected to be small and closed, the boundary-layer equations were applied.

It is obvious that the transport equations for heat (17) and mass (18) are similar. This results from the following assumptions:

- the components of the binary mixture are non-reacting;
- there are no internal heat or mass sources;
- the boundary conditions are similar, which is the case for an isothermal wall;
- the saturation pressure of the sublimating component is low.

Since one purpose of this investigation is to prepare the experimental study of the mass transfer in the pipe applying the naphthalene sublimation technique (presented in part II), it can be stated that the restrictions introduced above can also be fulfilled in the experiments. The mass transfer in this system is described by equation (18), using a Schmidt number of $Sc = 2.5$.

3. NUMERICAL SOLUTION

For the numerical solution of equations (12)–(18) the following dimensionless variables were introduced:

$$u^* = \frac{u}{U_m} \quad v^* = \frac{v}{U_m}\sqrt{Re_{dm}} \quad p^* = \frac{p}{\rho U_m^2}$$

$$k^* = \frac{k}{U_m^2} \quad \varepsilon^* = \frac{r_m \varepsilon}{U_m^3} \tag{24}$$

$$g^* = \frac{T - T_0}{T_w - T_0} \quad c^* = \frac{c - c_0}{c_w - c_0} \tag{25}$$

$$x^* = \frac{x}{r_m} \quad y^* = \frac{y}{r_m}\sqrt{Re_{dm}}. \tag{26}$$

Further, use was made of the Mangler transformation to supress the singularity at the centerline of the pipe:

$$u^* = \bar{u} \quad v^* = \frac{1}{(y^*)^i}\bar{v} \tag{27}$$

$$\mathrm{d}x^* = \mathrm{d}\bar{x} \quad (y^*)^i \mathrm{d}y^* = \mathrm{d}\bar{y}. \tag{28}$$

In a final transformation step the streamfunction was introduced and the coordinate lines were transformed to match the pipe geometry, for an easier application of the boundary conditions:

$$\delta = \frac{r_w(x)}{r_m} \tag{29}$$

$$\bar{u} = \frac{\partial}{\partial \bar{y}}(-\delta^2 F) \quad \bar{v} = -\frac{\partial}{\partial \bar{x}}(-\delta^2 F) \tag{30}$$

$$y_0 = \frac{\sqrt{Re_{dm}}}{(i+1)} - \frac{\bar{y}}{\delta^{(i+1)}} \quad x_0 = \bar{x}. \tag{31}$$

Successively applying the transformations mentioned above to equations (12)–(23) leads to the following set of equations:

$$\frac{\partial F}{\partial y_0}\frac{\partial k^*}{\partial x_0} - \frac{\partial F}{\partial x_0}\frac{\partial k^*}{\partial y_0} - \frac{i+1}{\delta} F \frac{\partial \delta}{\partial x_0}\frac{\partial k^*}{\partial y_0}$$

$$= \frac{1}{\delta^{2(i+1)}}\frac{\partial}{\partial y_0}\left[(y^*)^{2i}\left(1 + \frac{v_t}{v\sigma_k}\right)\frac{\partial k^*}{\partial y_0}\right]$$

$$+ \frac{v_t}{v}\frac{1}{\delta^{2(i+1)}}(y^*)^{2i}\left(\frac{\partial^2 F}{\partial y_0^2}\right)^2 - \varepsilon^* \tag{32}$$

$$\frac{\partial F}{\partial y_0}\frac{\partial^2 F}{\partial x_0 \partial y_0} - \frac{\partial F}{\partial x_0}\frac{\partial^2 F}{\partial y_0^2} - \frac{(i+1)}{\delta} F \frac{\partial \delta}{\partial x_0}\frac{\partial^2 F}{\partial y_0^2}$$

$$= -\frac{\partial p}{\partial x_0} + \frac{1}{\delta^{2(i+1)}}\frac{\partial}{\partial y_0}\left[(y^*)^{2i}\left(1 + \frac{v_t}{v}\right)\frac{\partial^2 F}{\partial y_0^2}\right] \tag{33}$$

$$\frac{\partial p}{\partial y_0} = 0 \tag{34}$$

$$\frac{\partial F}{\partial y_0}\frac{\partial \varepsilon^*}{\partial x_0} - \frac{\partial F}{\partial x_0}\frac{\partial \varepsilon^*}{\partial y_0} - \frac{(i+1)}{\delta} F \frac{\partial \delta}{\partial x_0}\frac{\partial \varepsilon^*}{\partial y_0}$$

$$= \frac{1}{\delta^{2(i+1)}}\frac{\partial}{\partial y_0}\left[(y^*)^{2i}\left(1 + \frac{v_t}{v\sigma_\varepsilon}\right)\frac{\partial \varepsilon^*}{\partial y_0}\right]$$

$$+ f_1 C_1 \frac{v_t}{v}\frac{1}{\delta^{2(i+1)}}(y^*)^{2i}\left(\frac{\partial^2 F}{\partial y_0^2}\right)^2 - f_2 C_2 \frac{(\varepsilon^*)^2}{k^*} \tag{35}$$

$$\frac{\partial F}{\partial y_0}\frac{\partial g^*}{\partial x_0} - \frac{\partial F}{\partial x_0}\frac{\partial g^*}{\partial y_0} - \frac{(i+1)}{\delta} F \frac{\partial \delta}{\partial x_0}\frac{\partial g^*}{\partial y_0}$$

$$= \frac{1}{Pr}\frac{1}{\delta^{2(i+1)}}\frac{\partial}{\partial y_0}\left[(y^*)^{2i}\left(1 + \frac{Pr v_t}{Pr_t v}\right)\frac{\partial g^*}{\partial y_0}\right] \tag{36}$$

$$\frac{\partial F}{\partial y_0}\frac{\partial c^*}{\partial x_0} - \frac{\partial F}{\partial x_0}\frac{\partial c^*}{\partial y_0} - \frac{(i+1)}{\delta} F \frac{\partial \delta}{\partial x_0}\frac{\partial c^*}{\partial y_0}$$

$$= \frac{1}{Sc}\frac{1}{\delta^{2(i+1)}}\frac{\partial}{\partial y_0}\left[(y^*)^{2i}\left(1 + \frac{Sc v_t}{Sc_t v}\right)\frac{\partial c^*}{\partial y_0}\right] \tag{37}$$

with

$$y^* = \delta\left[1 - \frac{(i+1)y_0}{\sqrt{Re_{dm}}}\right]^{1/(i+1)} \tag{38}$$

$$Re_t = \frac{(k^*)^2}{\varepsilon^*} Re_{dm} \tag{39}$$

$$Re_k = \delta Re\left[1 - \left(1 - \frac{(i+1)y_0}{\sqrt{Re_{dm}}}\right)^{1/(i+1)}\right]\sqrt{k^*} \tag{40}$$

and with the boundary conditions at the wall

$$y_0 = 0: \quad F = 0 \quad \frac{\partial F}{\partial y_0} = 0, \quad k^* = 0 \quad \varepsilon^* = \frac{1}{\delta^2}\frac{\partial^2 k^*}{\partial y_0^2} \tag{41}$$

$$g^* = 1 \quad c^* = 1 \tag{42}$$

and at the centerline

$$y_0 = \frac{\sqrt{Re}}{i+1}: \quad \frac{\partial^2 F}{\partial y_0^2} = 0 \quad \frac{\partial k^*}{\partial y_0} = 0$$

$$\frac{\partial \varepsilon^*}{\partial y_0} = 0 \quad \frac{\partial g^*}{\partial y_0} = 0 \quad \frac{\partial c^*}{\partial y_0} = 0 \tag{43}$$

$$F = \frac{\sqrt{Re_{dm}}}{(i+1)\,\delta^{i+1}}. \tag{44}$$

Chieng and Launder [8] as well as Yap [9] found that the LRN k–ε models predict heat transfer rates in a pipe with a sudden expansion in the vicinity of the reattachment point, up to seven times higher than measured values. The reason for this problem is the attribute of the LRN model to yield an excessive level of the near wall length scales.

In an attempt to cure this problem, Yap added an additional source term S_ε to the right hand side of the ε-equation (35):

$$S_\varepsilon = \mathrm{Max}\left[0.83\frac{\varepsilon^2}{k}\left(\frac{l}{C_l n}-1\right)\left(\frac{l}{C_l n}\right), 0\right] \tag{45}$$

with

$$l = \frac{k^{3/2}}{\varepsilon} \tag{46}$$

$C_l = 2.4$ and 'n' the normal distance to the wall. In case of a flow with local equilibrium the source term S_ε vanishes because

$$C_l n = \frac{k^{3/2}}{\varepsilon}. \tag{47}$$

In non-equilibrium flow the term acts to reduce the departure of the turbulent length scale from its local equilibrium value.

Since separated flows as well as reattachment points are expected in the flow through a pipe with sinusoidally varying diameter, the Yap correction was applied in this study. In laminar flow the resulting equations were solved using the Keller–Box method. Whereas in turbulent flow an implicit algorithm was applied, which provides more stability.

To overcome the numerical instabilities in regions with reversed flow, the FLARE-approximation [10] was introduced. With the use of this approximation the convective term in the axial direction, which is normally small, is neglected. The use of up to 140 nodes in the radial direction and 300 nodes in the axial direction for turbulent flow was necessary to achieve a grid independent solution. The equations were solved on a nonuniform grid, with finer grid spacing near the wall and contraction in the axial direction near points of vanishing wall shear stress.

An iterative method was used to solve the coupled nonlinear set of equations, applying Newton's linearisation method. Iterations were continued until the difference between the two last solutions was less than 10^{-8}. To start the algorithm fully developed flow conditions with a homogeneous temperature and concentration distribution for a pipe with constant diameter were assumed. For further stabilisation of the numerical algorithm, especially in turbulent flow, underrelaxation factors of 0.7–0.3 were used.

4. RESULTS

In the following section the results of the calculations, using the equations and methods introduced above, will be discussed. In the first part typical flow regimes from laminar to transitional and turbulent flow and the resulting distribution of the Nusselt and Sherwood numbers are discussed. The results were calculated for a fixed geometry which is given by a sinus function:

$$\delta(x^*) = 1 - \gamma_h \sin\left(\frac{2\pi}{\gamma_\lambda}x^*\right). \tag{48}$$

In the second part the influence of the different flow and geometry parameters on the Nusselt and Sherwood number will be outlined.

4.1. *Laminar flow*

Figure 2 shows the distribution of the axial velocity at different locations downstream in one wave of the pipe for $Re_{dm} = 300$ and fully developed flow conditions. The profile in the narrowest cross-section shows a larger wall velocity gradient compared to the parabolic profile of the flow through a straight pipe. Moving downstream into the diverging part of the pipe, the axial pressure gradient changes its sign from negative to positive which causes a flow separation and the development of flow reversal in the bulge part of the pipe. In the converging part the axial pressure gradient changes its sign again, causing the reattachment of the flow.

In Fig. 3 the streamlines for one wavelength are depicted for $Re_{dm} = 300$, elucidating how flow separation and reattachment in one wave of the pipe lead to

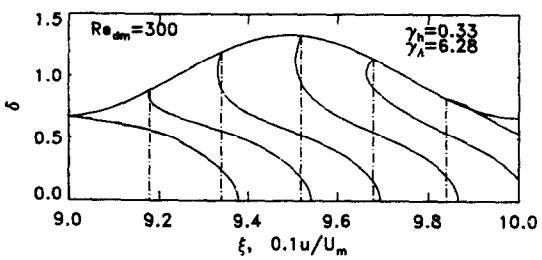

Fig. 2. Axial velocity profiles for fully developed laminar flow, $Re_{dm} = 300$.

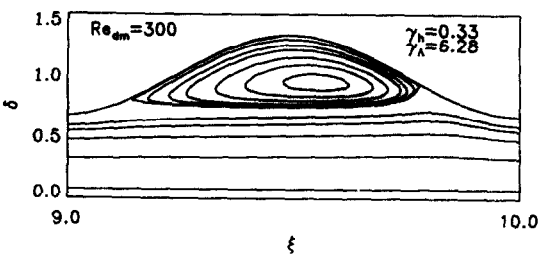

Fig. 3. Streamlines for $Re_{dm} = 300$, $\gamma_h = 0.333$ and $\gamma_\lambda = 6.28$.

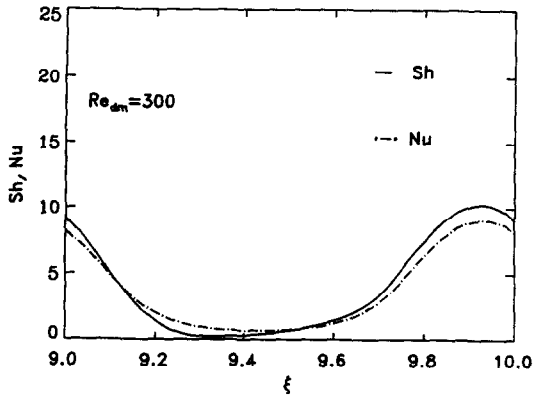

Fig. 4. Sherwood and Nusselt numbers for $Re_{dm} = 300$, $\gamma_h = 0.333$ and $\gamma_A = 6.28$.

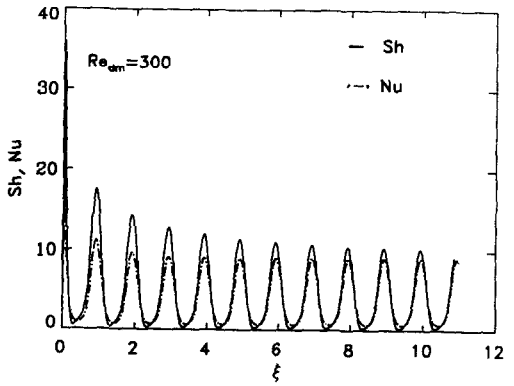

Fig. 7. Sherwood and Nusselt numbers as a function of the pipe length (11 waves) for $Re_{dm} = 300$, $\gamma_h = 0.333$ and $\gamma_A = 6.28$.

a closed separation bubble in the bulge part. Figure 4 shows the resulting distribution of the calculated Nusselt and Sherwood numbers in the same wave. The increasing wall velocity gradient in the narrowest cross section causes a very thin concentration and thermal boundary-layer, resulting in growing Nusselt and Sherwood numbers. Near the reattachment points, where high velocity components normal to the wall occur, the boundary-layer thickness is additionally reduced, leading to a maximum of the convective heat and mass transfer coefficients downstream of the reattachment point. Since in attached flow the convective boundary-layer thickness is reciprocal to the Prandtl and Schmidt numbers, the Sherwood number is larger than the Nusselt number. Figures 5 and 6 show the distribution of the isotherms and the lines of constant concentration. It is obvious that the concentration boundary-layer separates together with the main flow, leading to a greater thickness locally, compared to the thermal boundary layer. This is due to less diffusivity in the concentration field and leads to the fact that the Sherwood number is smaller than the Nusselt number at this location.

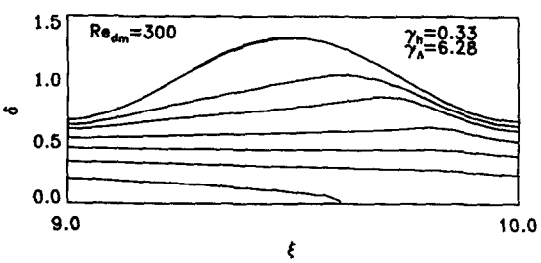

Fig. 5. Isotherms for $Re_{dm} = 300$, $\gamma_h = 0.333$ and $\gamma_A = 6.28$.

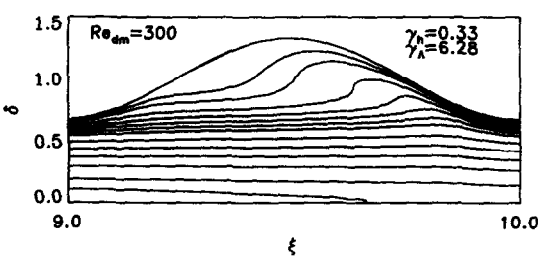

Fig. 6. Concentration field for $Re_{dm} = 300$, $\gamma_h = 0.333$ and $\gamma_A = 6.28$.

At the reattachment point a second boundary layer, which has an opposite direction to the mainflow, develops into a separation bubble. In this secondary flow normal conditions hold, with a thinner concentration boundary-layer compared to the thermal boundary layer. Thus, the Sherwood number has higher values than the Nusselt number.

Figure 7 shows that the maxima of the Sherwood and Nusselt numbers decay exponentially with the pipe length, in this case covering 11 sinusoidal waves.

4.2. *Transitional flow*

The range of Reynolds number for the transitional flow regime in the sinusoidal pipe is as yet unknown. But the studies of Nishimura *et al.* [2–4] carried out in a plane channel with sinusoidal walls exhibiting the typical features of turbulent flow, such as large vortex structures and increasing convective transport, can be observed for Reynolds numbers much lower than those for a plane channel. They observed the first indications of transitional flow at Reynolds numbers above $Re_{dm} = 600$.

With increasing Reynolds number and hence, increasing axial velocity for a fixed geometry and fluid properties, the shear layer separating the main flow from the recirculation bubble in the bulge part of the pipe becomes unstable due to the high shear stresses. These shear stresses occur in a layer separating the main flow region with large positive axial velocity components from the recirculating bubble with low negative axial velocity components. The growth of small inlet disturbances in these shear layers is similar to the so called Kelvin–Helmholtz instability, described in ref. [11] for a plane unbounded shear flow.

Under these conditions the flow is time dependent, with large vortex structures separating from the shear layer and flowing downstream through the pipe. Since the numerical algorithm described in Section 3 is

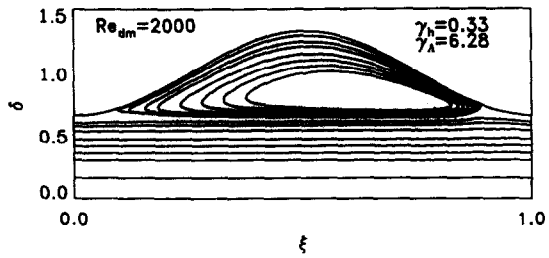

Fig. 8. Streamlines for $Re_{dm} = 2000$, $\gamma_h = 0.333$ and $\gamma_A = 6.28$ (laminar flow).

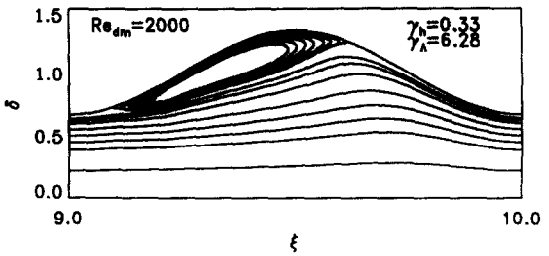

Fig. 10. Streamlines for $Re_{dm} = 2000$, $\gamma_h = 0.333$ and $\gamma_A = 6.28$ (turbulent flow).

developed for a steady flow conditions, no simulation of this flow structure was possible. The implemented LRN k–ε model allows the calculation of the time average flow-, temperature- and concentration-fields.

To discuss the flow structure under transitional flow conditions the following scenario is developed: at a Reynolds number of about $Re_{dm} = 2000$, which is near the critical Reynolds number for a straight pipe, the flow in the entrance region of the sinusoidal pipe is still laminar. Therefore, to calculate the flow field as well as heat and mass transfer no turbulence model was applied. Figure 8 depicts the calculated streamlines and Fig. 9 the predicted Sherwood and Nusselt numbers for $Re_{dm} = 2000$. The flow field is similar to that calculated for $Re_{dm} = 300$ but with a larger recirculation bubble, and hence, an increased axially extended region of low convective heat and mass transfer. As explained above, the unstable shear layers separating the recirculating flow from the main flow field, feed energy to the most unstable modes in the flow, causing small disturbances to grow. These growing disturbances lead to a periodical breakdown of the recirculation bubbles and the resulting vortices flow downstream. Following the assumption of the well known energy cascade in turbulent flow, these vortices split up into an extended number of smaller vortices which then lose their energy by dissipation, which is typical of turbulent flow. Therefore, it seems fair to assume that after a reasonable length downstream from the entrance the flow field can be simulated applying the presented LRN turbulence model.

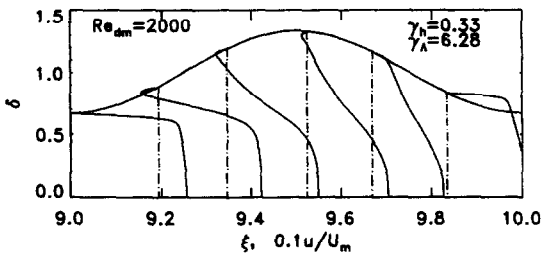

Fig. 11. Axial velocity profiles for $Re_{dm} = 2000$, $\gamma_h = 0.333$ and $\gamma_A = 6.28$ (turbulent flow).

Figures 10 and 11 show the calculated streamlines and axial velocity profiles. In Fig. 12 the resulting distribution of the Nusselt and Sherwood numbers is plotted for one wavelength. Due to the Reynolds stresses in turbulent flow, the axial velocity profiles show a higher velocity gradient at the wall, which results in a reduced size of the recirculation bubble and a reduced axial extension of the minimum in the Sherwood and Nusselt number's distribution in the bulge part of the pipe. The shear stresses in the shear layer lead to an increasing production of turbulent kinetic energy and a reduced thickness of the diffusion dominated layer near the wall, which is the main transport resistance. This causes an increase in convective transport some distance downstream of the separation point, which leads to a maximum in the Sherwood and Nusselt numbers. A further rise of the Sherwood and Nusselt numbers can be observed near the reattachment point, where the thickness of the thermal and concentration boundary layer is reduced again.

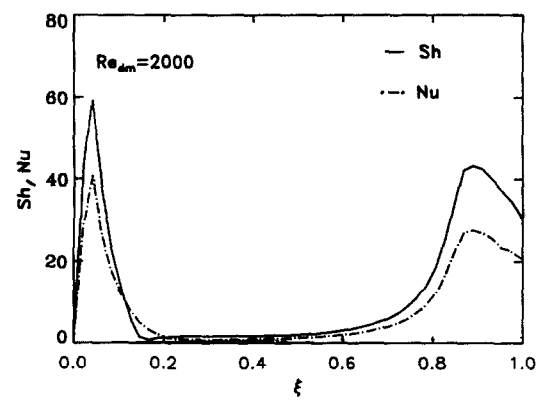

Fig. 9. Sherwood and Nusselt numbers for $Re_{dm} = 2000$, $\gamma_h = 0.333$ and $\gamma_A = 6.28$ (laminar flow).

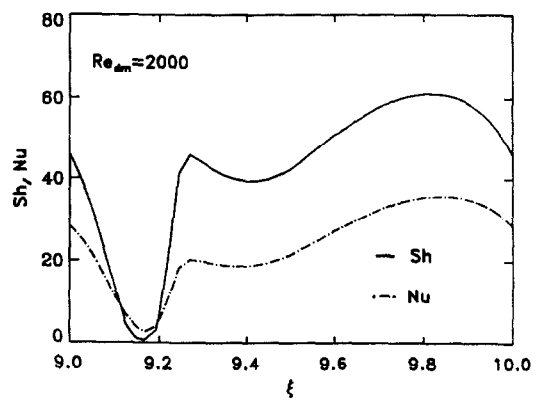

Fig. 12. Sherwood and Nusselt numbers for $Re_{dm} = 2000$ in the tenth wave, $\gamma_h = 0.333$ and $\gamma_A = 6.28$ (turbulent flow).

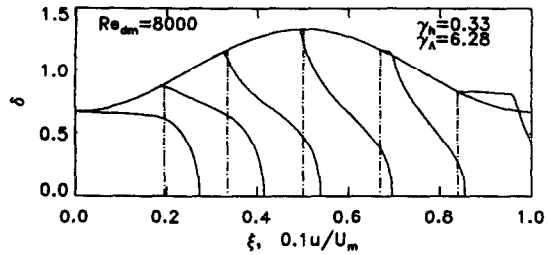

Fig. 13. Axial velocity profiles for $Re_{dm} = 8000$, $\gamma_h = 0.333$ and $\gamma_A = 6.28$.

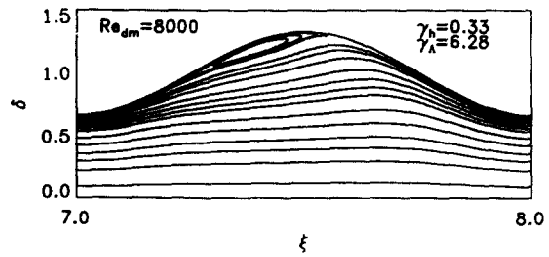

Fig. 15. Streamlines for $Re_{dm} = 8000$, $\gamma_h = 0.333$ and $\gamma_A = 6.28$ (fully developed).

and hence, the temperature and concentration gradient at the wall are increased. For a detailed analysis of the transient flow regime, the reader is referred to Part II.

4.3. *Turbulent flow*

With further increased Reynolds numbers the flow entering the sinusoidal pipe is assumed to be turbulent at the entrance. Figure 13 shows the axial velocity profiles for $Re_{dm} = 8000$ in the first wave. Due to the higher velocity gradients and hence, an increased kinetic energy of the fluid near the wall, the fluid is able to flow further into the diverging part of the wave without separation. However, Fig. 14 elucidates that the radial and axial extension of the recirculation bubble is reduced compared to that for laminar flow. It can be observed that the flow separates at point 'A', but the resulting separation bubble is very thin. It must be assumed that in reality the flow in this area is very unstable with frequent separation of small vortices. The real flow would show stationary recirculation solely in the area where the calculated streamlines show a remarkable size of separation bubble. As discussed previously for transitional flow, in turbulent flow the shear layers promote the production of turbulence which causes a reduction in the size of the separation bubble, as shown in Fig. 15 for fully developed turbulent flow.

In turbulent flow the convective heat and mass transfer are strongly affected by the flow field and the turbulence structure. Therefore, it is necessary to discuss in addition to the flow field the characteristics of the turbulence in order to understand the calculated Sherwood and Nusselt numbers depicted in Fig. 16 for fully developed flow ($Re_{dm} = 8000$). The sharp minimum of the Sherwood and Nusselt numbers in the

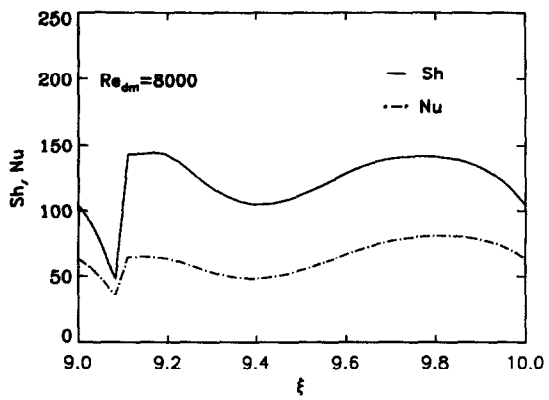

Fig. 16. Sherwood and Nusselt number for $Re_{dm} = 8000$ in the tenth wave, $\gamma_h = 0.333$ and $\gamma_A = 6.28$.

diverging part of the wave is caused by the increasing thickness of the temperature and concentration boundary layer near the separation point. The large radial velocity gradients in the developing separation bubble very close to the wall cause a peak of Reynolds stresses in the near wall region, as depicted in Fig. 17. The high Reynolds stresses and, hence, the increased turbulence diminish the thickness of the viscous sublayer, thus increasing the wall gradients of the temperature and concentration profiles, which leads to a peak in the Sherwood and Nusselt numbers shortly behind the point of separation. From a more physical point of view it can be said that the increased near wall turbulence reduces the viscous sublayer and hence, the thickness of the diffusion dominated layer near the wall which is the main transport resistance is also reduced, thus causing a peak in the Sherwood and Nusselt numbers' profile.

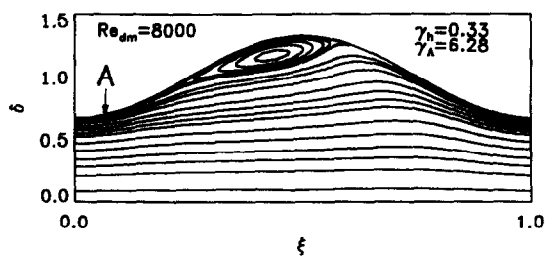

Fig. 14. Streamlines for $Re_{dm} = 8000$, $\gamma_h = 0.333$ and $\gamma_A = 6.28$ (entrance region).

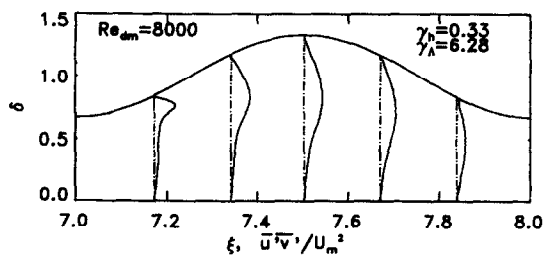

Fig. 17. Reynold's stresses for $Re_{dm} = 8000$, $\gamma_h = 0.333$ and $\gamma_A = 6.28$.

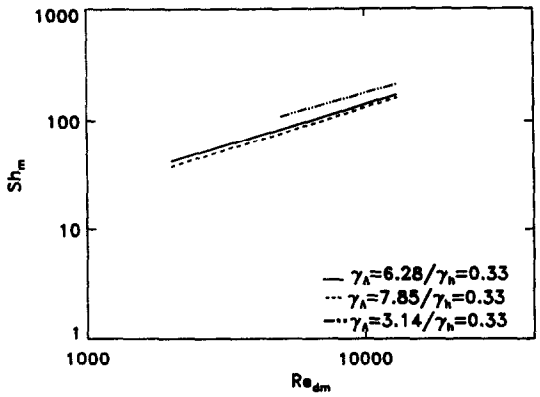

Fig. 18. Mean Sherwood number per wavelength for various geometry parameters γ_A (fully developed turbulent flow).

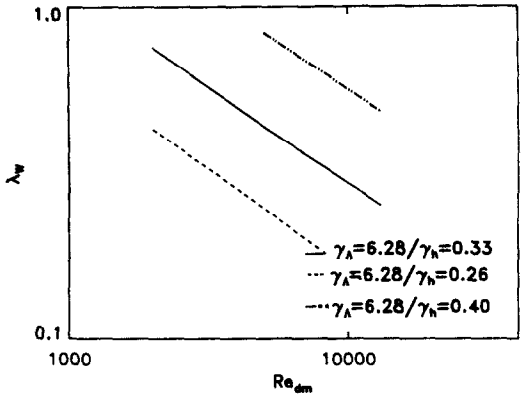

Fig. 20. Mean friction coefficient per wavelength for various geometry parameters γ_h (fully developed turbulent flow).

4.4. *Parameter variation*

The purpose of this section is, to investigate the influence of different parameters on the solution, except for that of the Prandtl and Schmidt numbers since this was already included in the foregoing discussion on the temperature and concentration fields due to the similarity of the transport equations. The calculations were performed with $Pr = 0.7$ and $Sc = 2.5$, respectively.

Therefore, it seems to be reasonable to confine the discussion to the mean Sherwood number per wavelength for fully developed conditions and varying the parameters γ_A, γ_h and Re_{dm}. In addition we restrict the discussion to turbulent flow regimes because of their higher practical importance compared to laminar flow. Figure 18 shows the mean Sherwood number per wavelength in turbulent flow as a function of the Reynolds number for different γ_A. The variation of γ_h is given in Fig. 19. From both figures the conclusion can be drawn that the heat and mass transfer is enhanced by increasing values of γ_h and decreasing γ_A. The main reason for this behaviour is the growing ratio γ_h/γ_A of the pipe wall function, resulting in increasing velocity components normal to the wall near the reattachment point. This is comparable to the impingement of a jet on a wall.

In addition to the convective transport the numerical analysis reveals that the pressure drop over one wavelength is increased considerably by growing values of γ_h, as shown in Fig. 20.

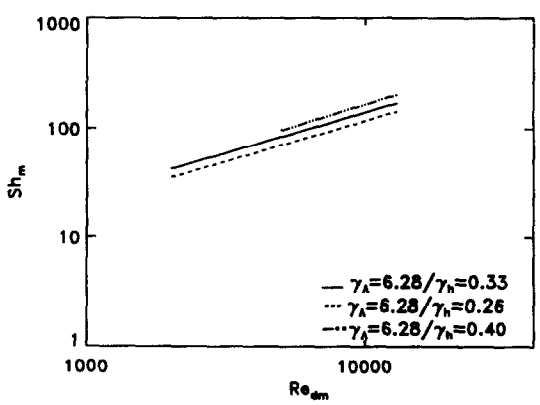

Fig. 19. Mean Sherwood number per wavelength for various geometry parameters γ_h (fully developed turbulent flow).

5. SUMMARY

A numerical study was performed to investigate the effect of wavy walls on the convective transport in pipe flow. The basis of the investigations are the momentum and transport equations for heat and mass transfer written in boundary-layer form. For laminar flow the results show a reduced convective transport in the bulge part of the pipe where the streamlines visualize a closed separation bubble. A maximum of the Nusselt and Sherwood numbers was calculated near the reattachment point of the flow in the converging part of the wave. The mean convective transport over one wave for fully developed flow is nearly the same as that for a straight pipe.

With increasing Reynolds number the flow becomes unstable and for $Re_{dm} = 2000$ the results of the calculation applying the LRN turbulence model, introduced by Lam and Bremhorst, show a reduced size of the separation bubble compared to laminar flow. This is an effect of increased shear stresses in the layer separating the recirculation bubble from the main flow which augment the Reynolds stresses. With the growth of the turbulence level the convective transport is improved, resulting in higher Nusselt and Sherwood numbers compared to a straight pipe. The local distribution of the convective transport in turbulent flow over one wave shows a sharp maximum near the separation point in the diverging part and a second maximum near the reattachment point. in between is a minimum caused by the separating bubble.

A parameter study shows that the gradient of the wall function is proportional to the calculated Nusselt and Sherwood numbers in turbulent flow.

REFERENCES

1. Sparrow, E. M. and Prata, A. T., Numerical solution for laminar flow and heat transfer in a periodically con-

verging–diverging tube, with experimental confirmation. *Numerical Heat Transfer*, 1983, **6**, 441–461.
2. Nishimura, T., Ohori, Y. and Kawamura, Y., Flow characteristics in a channel with symmetric wavy wall for steady flow. *Journal of Chemical Engineering of Japan*, 1984, **17**, 466–471.
3. Nishimura, T., Ohori, Y., Kajimoto, Y. and Kawamura, Y., Mass transfer characteristics in a channel with symmetric wavy wall for steady flow. *Journal of Chemical Engineering of Japan*, 1985, **18**, 550–555.
4. Nishimura, T., Kajimoto, Y. and Kawamura, Y., Mass transfer enhancement in channels with a wavy wall. *Journal of Chemical Engineering of Japan*, 1986, **19**, 142–144.
5. Greiner, M., Chen R.-F. and Wirtz, R. A., Heat transfer augmentation through wall-shape-induced flow destabilization. *Journal of Heat Transfer*, 1990, **112**, 336–341.
6. Lam, C. K. G. and Bremhorst, K., A modified form of the k–ε model for predicting wall turbulence. *Journal of Fluids Engineering*, 1981, **103**, 456–460.
7. Anderson, D. A., Tannehill, J. C. and Pletcher, R. H., *Computation Fluid Mechanics and Heat Transfer*. McGraw–Hill, New York 1984.
8. Chieng, C. C. and Launder, B. E., On the calculation of turbulent heat transport downstream from an abrupt pipe expansion. *Numerical Heat Transfer*, 1980, **3**, 189–207.
9. Yap, C. R., Turbulent heat and momentum transfer in recirculating and impinging flows. Ph.D. thesis, Faculty of Technology, University of Manchester, Manchester, 1987.
10. Reyhner, T. A. and Flügge-Lotz, I., The interaction of a shock wave with a laminar boundary layer. *International Journal of Nonlinear Mechanics*, 1968, **3**, 173–199.
11. Lesieur, M., *Turbulence in Fluids*, 2nd edn. Kluwer Academic, Dordrecht, 1990.